EXPERIMENTAL INVESTIGATION OF NEGATIVELY BUOYANT SEDIMENT PLUMES RESULTING FROM DREDGING OPERATIONS

BOUDEWIJN DECROP [1,4], TOM DE MULDER [3], PETER TROCH [3], ERIK TOORMAN [2] & MARC SAS [4]

[1] *Hydraulics Laboratory, Ghent University, Sint-Pietersnieuwstraat 41, Ghent, B-9000, Belgium. Boudewijn.Decrop@ugent.be*

[2] *Professor, Hydraulics Laboratory, KULeuven Kasteelpark Arenberg 40, Heverlee, B-3001, Belgium. Erik.Toorman@bwk.kuleuven.be*

[3] *Professor, Hydraulics Laboratory, Dept. of Civil Engineering, Ghent University, Sint-Pietersnieuwstraat 41, Ghent, B-9000, Belgium.*

[4] *IMDC, Coveliersstraat 15, Antwerp, B-2600, Belgium.*

Abstract

In a first step to investigate the behaviour of sediment plumes released from dredging vessels, an experimental facility has been built to release scaled fine sediment plumes in the presence of cross flow. High-frequency measurements of velocity components and sediment concentration are obtained using acoustic and optical backscatter instruments. The paths of the axis of the experimental buoyant plumes in cross-flow have been compared to integral laws by Fisher *et al.* (1979), showing relatively good agreement for plumes not influenced by the dredger's hull. Plumes with low relative density difference and high crossflow to outflow velocity ratio deviate from the integral laws due to additional mixing induced by the hull boundary layer and wake.

1. Introduction

Dredging is an activity often related to economical expansion projects along the world's coastlines and has been strongly increasing for some years. In view of the increased attention to environmental impacts of coastal and offshore dredging operations, research in this field is on the rise.

In this context the effect of turbidity generated by dredging activities plays an important role. The sediments brought in suspension can generate effects ranging from reduced light penetration in the water column over burial of sea bed ecosystems to dispersion of toxic materials attached to polluted sediments (Dankers, 2002; Smith et al., 2008). The dispersion of benthic material can have other impacts including siltation of still water bodies such as bays, docks or harbours.

Sediments in highly-concentrated suspensions are released from the often used Trailing Suction Hopper Dredgers (THSD) through an overflow of the hopper. Depending on sediment concentration and ambient current velocity (relative to the sailing vessel) the flow can either behave as a density-driven, negatively buoyant jet or as a plume mixing fast with the seawater and therefore losing its buoyancy. In the first case the dynamic plume sinks to the seabed while part of the sediment is mixed into the water column, in the second case almost all fine sediment

is brought in suspension (Spearman et al., 2007). Both cases can lead to a large, non-buoyant, passive far-field plume with the potential to travel large distances due to advection with coastal or estuarine currents.

2. Methods

2.1 Experimental setup

An experimental facility has been built to investigate the release and behavior of scaled sediment plumes in the presence of cross flow (Figure 1). In a mixing tank fitted with a circulating pump (pump 1) a mixture of water and sediment is homogenised. Using a second pump (pump 2), the mixture is fed to a constant head vessel located on top of the flume. The constant head vessel is designed to keep a constant water level by being overtopped and leading the excess mixture back to the mixing tank. The constant head vessel is connected to an opening in a polycarbonate plate, serving as a schematized ship hull, situated at a 'draft' of 4 cm below the water level in the flume. The constant level in the vessel, combined with an orifice in the pipe guarantees for a constant, known discharge of the mixture with controlled sediment concentration into the flume. Fine sediment (kaolin clay) with a narrow particle size distribution has been used in order to minimise the effect of settling and particle size distributions and thus simplify the interpretation.

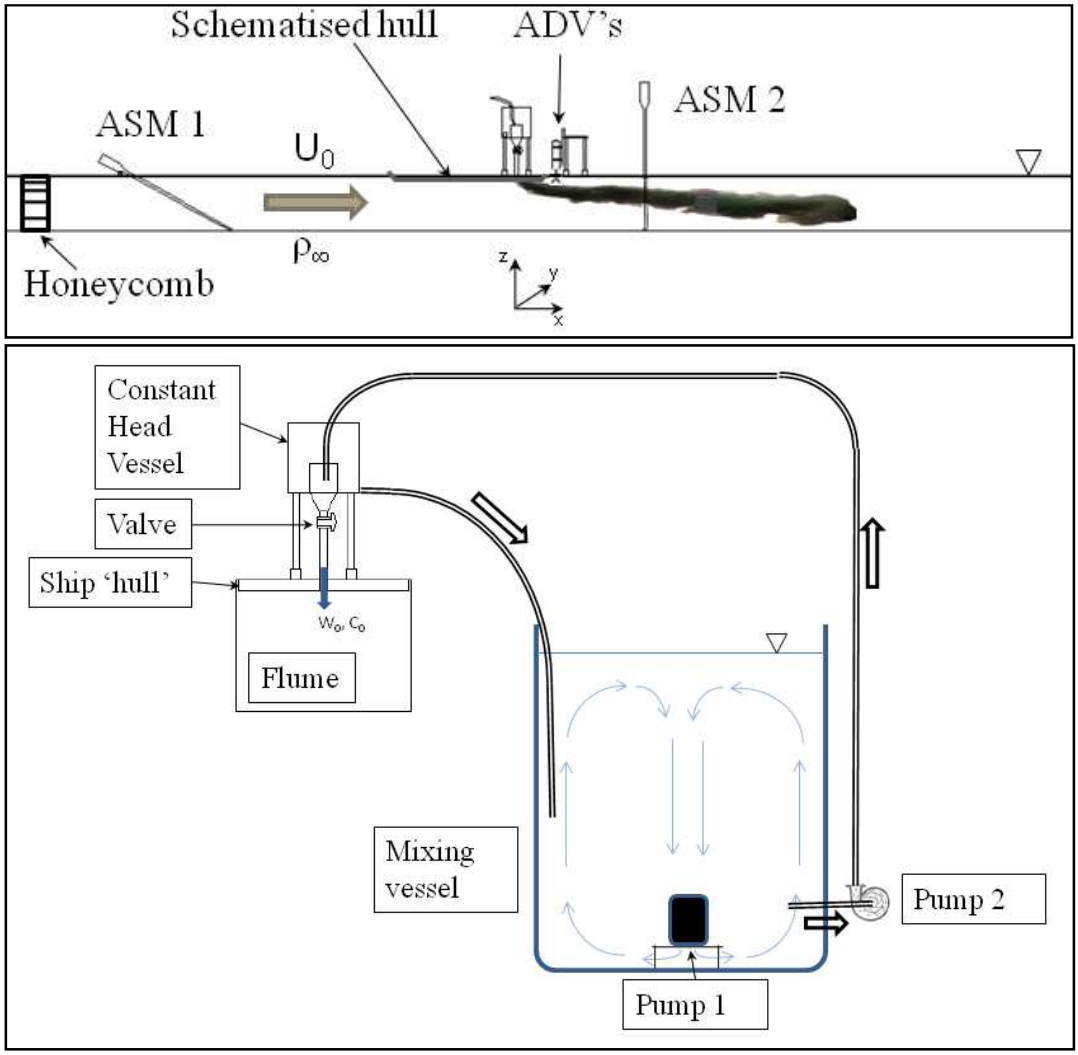

Figure 1. Experimental setup using two ADV and two ASM instruments. Configuration in the flume (top) and water-sediment mixture feeding mechanism (below).

High-frequency measurements of velocity components and sediment concentration are obtained using acoustic and optical backscatter equipment, still regarded as the best options to obtain information in highly turbid flows. The Acoustic Doppler Velocimeter (ADV) is used to provide mean and fluctuating velocity profiles by means of the Pulse Coherent Doppler technique. In this laboratory study, the instrument's acoustic backscatter intensity is calibrated a priori to measure the time-averaged sediment concentrations in the plume as well as turbulent fluctuations of the concentration allowing for the determination of turbulent sediment and momentum fluxes (e.g. Shabbir and Taulbee, 2000). The optical backscatter signal of an Argus Surface Meter (ASM) has been calibrated for the response in kaolin clay suspensions and has been installed to obtain additional profiles of mean sediment concentration at a higher spatial resolution.

By using a background of diffused white light and taking (high-speed) images, shadowgraphy measurement of the obscuration due to sediment allows the determination of the average elevation of the concentration maximum at any horizontal distance from the source up to about 2 m (32 to 60 pipe diameters, depending on the pipe).

2.2 Dynamic scaling

Dimensional analysis shows that two main dimensionless numbers represent force balances in the flow: the densimetric Froude number F_Δ and the velocity ratio λ.

$$F_\Delta = \frac{W_0}{\sqrt{gD\Delta\rho/\rho_\infty}} \quad [1]$$

$$\lambda = \frac{U_0}{W_0} \quad [2]$$

where W_0 is the initial vertical velocity at the start of the plume [m/s], U_0 the mean horizontal ambient velocity, to be interpreted as the vector sum of the current velocity and the vessel speed, D is the pipe diameter [m], $\Delta\rho = \rho_m - \rho_\infty$ with ρ_m the water-sediment mixture density [kg/m³] and ρ_∞ the ambient fluid mass density [kg/m³].

A third dimensionless number of importance is the pipe Reynolds number. Scaling both the Froude number and the Reynolds number leads to a unique solution of a scaling factor equal to one, which makes it impossible to scale on both dimensionless numbers. Therefore, the Reynolds number is not brought to scale but a minimum value of 4148 has been maintained in order to ensure turbulent pipe flow at the exit pipe.

The influence of mass density of the released material, exit velocity, pipe diameter and background current velocity are investigated. A total of 34 different experiments have been executed with F_Δ ranging from 0.24 to 9.15 and background to outflow velocity ratios between 0 and 8.7. In this way, dynamically scaled conditions have been produced corresponding to the range of conditions occurring while dredging in marine and coastal environments (Table 1). At this stage of the research, the influence of waves, air bubbles, propellers and intermittent discharges due to ship pitching are not taken into account.

Momentum length scales l_M ($=M_0^{3/4}B_0^{-1/2}$, with M_0 initial momentum flux and B_0 initial buoyancy flux) range from 0.23 to 8.56 pipe diameters, cross flow dominance lengthscales in jet regime z_M ($=M_0^{1/2}U_0^{-1}$) and in plume regime z_B ($=B_0\ U_0^{-1/3}$) range 0.01-2.4 and 0.1-2.6 pipe diameters respectively. Bent jet to bent plume distance z_C ($=z_M^{4/3}z_B^{-1}$) ranges 0.6-5.5 diameters.

Table 1. Ranges of dimensionless numbers and flow characteristics in both scaled (Lab.)and real life (R.L.) dimensions covered in the scaled experiment.

	F_Δ [-]	λ [-]	D [M]	U_0 [M/S]	W_0 [M/S]	ρ_m [kg/m^3]
MIN R.L.	0.24	0.0	1.26	0.0	0.5	1026
MAX R.L.	9.15	8.7	3.61	4.6	2.0	1221
MIN LAB.	0.24	0.0	0.034	0.0	0.11	1003
MAX LAB.	9.15	8.7	0.060	0.32	0.30	1031

2.3 Calibration for mean and turbulent fluctuations of sediment concentration

Both acoustic (ADV) and optical (ASM) backscatter instruments have been used to determine suspended sediment concentration in the plume. Both instruments have been submerged in the mixing vessel shown in Figure 1. Sediment concentration C is increased from 1 mg/l up to 20 g/l while recording instrument output for 2 minutes. At each concentration level a sample is taken close to the instruments' sampling volumes using a peristaltic pump.

ASM signals from each of the 144 individual optical backscatter sensors have been fitted to a quadratic calibration curve linking backscatter intensity to suspended sediment concentration. A selection of 16 out of the 144 calibration curves obtained in this way is shown in Figure 2 (right). The sensors show a similar shape of calibration curve but the offset at minimal sediment concentration is at a different level of optical backscatter intensity for each sensor resulting in 144 different calibration curves. ASM output showed saturation at about 1.2 g/l in this type of fine sediment for all sensors. The homogeneous mixture and the narrow grain size distribution of the sediment allows for a very clean calibration of the optical backscatter intensity. For all sensors, the coefficient of determination is at least 0.98.

The calibration range for sediment concentration obtained for the ADV sensor has been optimized by analyzing the instrument output for a wide variation of instrument settings such as power level, acoustic pulse length, sampling volume height. In this way the calibration range can be increased by a large factor (Salehi, 2009 and 2011), while avoiding disturbance of velocity measurement quality. In this study the difference in calibration ranges obtained after optimization is equal to a factor ten (Decrop *et al.*, 2012).

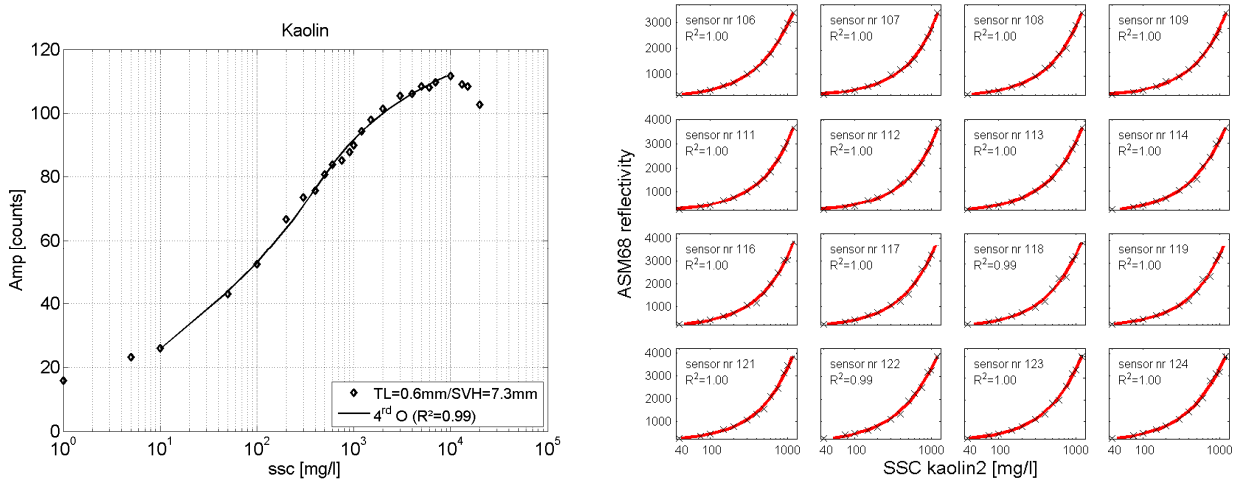

Figure 2. Instrument calibration curves for both ADV (left) and ASM (right).

Using optimal instrument settings a 4th order calibration curve is obtained, yielding $log_{10}(C)$ as a function of AMP, the amplitude of the backscattered acoustic signal. By subtracting

the average frequency spectrum of the ADV backscatter in uniform, still mixtures at different sediment concentration, a spectral correction can be performed on the high frequency (25 Hz) suspended sediment concentration signal. In this way, turbulent sediment diffusion fluxes in the plume can be resolved as well as Reynolds stresses (Decrop *et al.*, 2012).

2.4 Profile imaging

Images were taken at high sampling frequency (5 Hz) of the plume's vertical outline. A background of diffuse white light is used for contrast with the fringes of the plume (Figure 3). A minimum of 600 images per experiment have been used to compute fields of average and variance of light obstruction on a vertical plane across the plume centerline. Obscuration α has been computed at each pixel as follows:

$$\alpha_{i,j} = \frac{B_{i,j} - I_{i,j}}{B_{i,j}} \quad [1]$$

where, $B_{i,j}$ is the reference background light intensity, measured before the start of the experiment, $I_{i,j}$ is the light intensity measured during the plume experiment and i,j are the horizontal and vertical pixel indices.

Images have been corrected for horizontal and vertical perspective deformation and for light refraction at an air-water interface, neglecting the intermediate refraction due to the 15 mm glass panels.

Light obscuration profiles are not used as a direct estimator of sediment concentration due to multiple scattering, but to determine the plume trajectory and width as function of horizontal distance (Figure 3, right panels). Assuming the average obscuration is a measure of the integrated concentration C over the y-direction, it can be proven that if a section of the plume with a vertical plane has a Gaussian *C*-profile, the obscuration profile's Gaussian half-width equals the 3D half-width.

Additionally, the standard deviation of the obscuration at each position gives the intermittency factor at the y=0 plane (axis definition in Figure **1**).

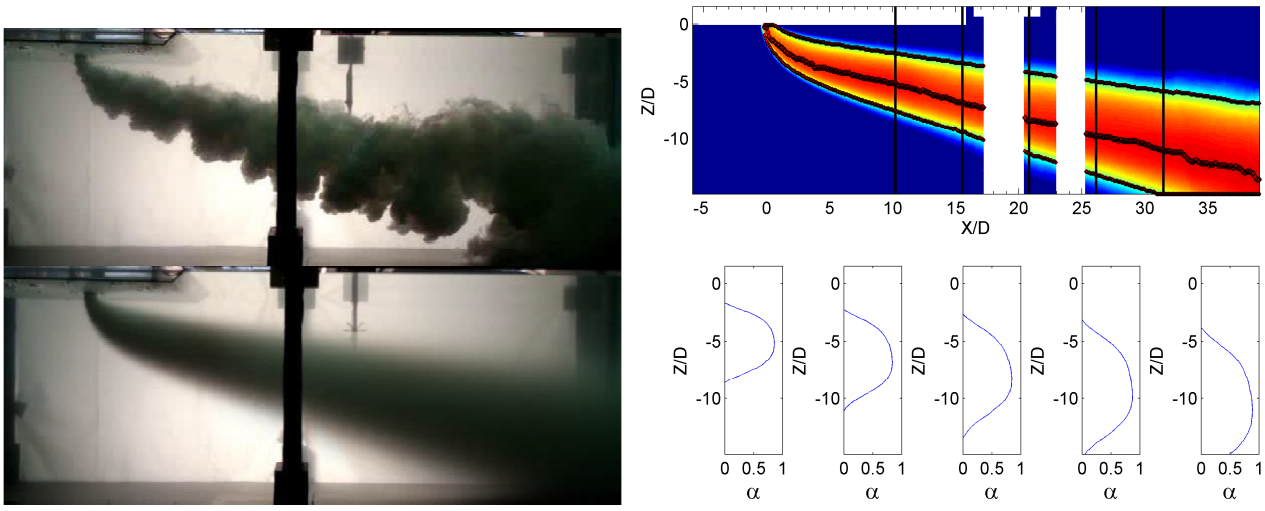

Figure 3. Image of a negatively buoyant sediment plume in cross flow. Upper left panel: instantaneous plume; Lower left panel: time-averaged image; Upper right panel: obscuration field with profile locations and plume axis/half-width; Lower right panel: vertical obscuration profiles at *x/D*=11, 16, 21, 26 and 32.

3. Results

3.1 Plume trajectory

Plume centrelines have been compared to integral laws by Fisher (1979) and to a Lagrangian model (Lee and Chu, 2003) for buoyant jets, showing the sediment plumes have substantially higher trajectories for higher values of λ (compare upper and lower panels in Figure 4). Both models have been derived based on two-fluid plumes, although this does not explain the difference to laboratory plume trajectories for high λ. Even though the Stokes number is small (St<<1, due to very fine sediment), it was observed in vertical plume tests that -unlike in passive tracer diffusion- the velocity half-width was not smaller than the concentration half-width. This would lead to a more narrow, denser plume with lower trajectory compared to two-fluid plumes. For plumes interacting with the boundary layer and the wake of the ship hull the difference in plume trajectory is obviously more pronounced for high λ values.

The observed difference compared with integrated buoyant jet models can be attributed to four possible effects: (i) entrainment of turbulent kinetic energy from the ambient flow, (ii) increased mixing due to the presence of the hull boundary layer, (iii) mixing due to the wake of the hull, starting at x/D=5 in the upper panel of Figure 4, (iv) increased mixing due to meandering of the plume, related to a Von Karman vortex street downstream of the vertical initial section of the plume.

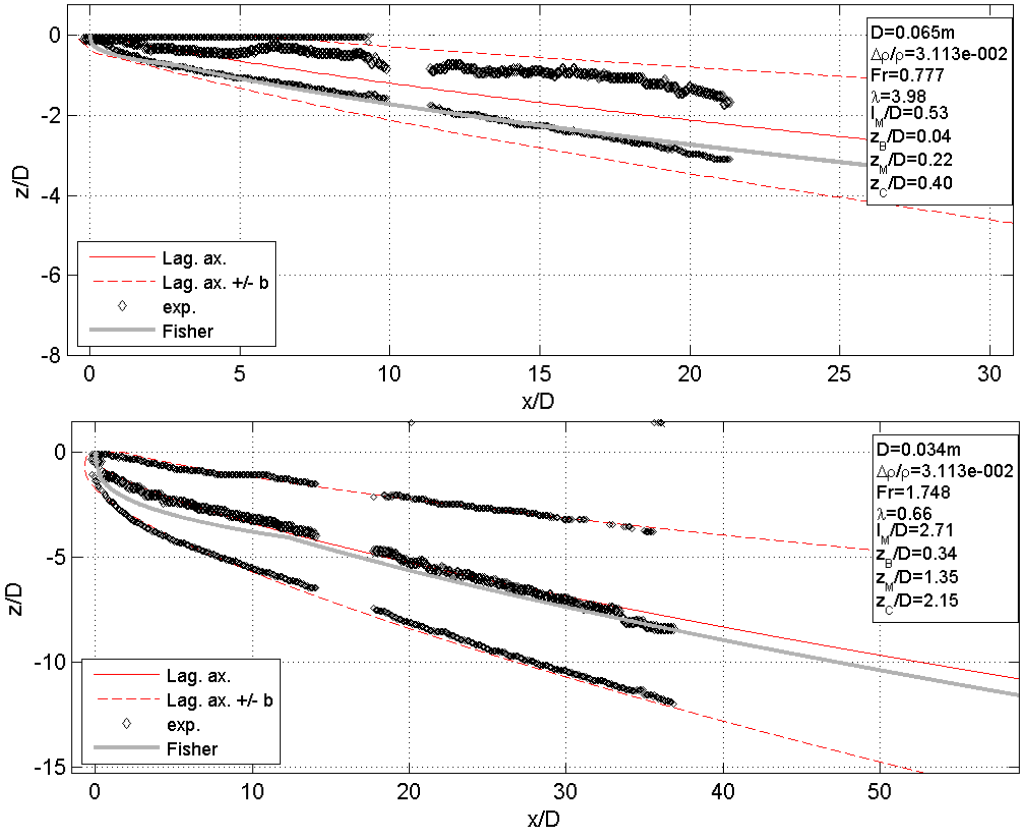

Figure 4. Experimental trajectories (axis and upper/lower half-width b shown) compared to asymptotic solutions by Fisher *et al.* (1979) and a Lagrangian model based on Lee & Chu (2003).

3.2 Mean quantities

Mean flow velocity in streamwise direction shows a profile in a plane of constant x in which the velocity beneath the plume is close to the background velocity. Above the plume the velocity is reduced due to blocking by the upstream part of the plume, which induces a wake. Velocity vectors (Figure 6) show clearly the typical counter-rotating vortex pair (Diez *et al.*, 2005).

Time-averaged sediment concentration is measured using both ADV and ASM. In both results the bimodal distribution caused by the counter-rotating vortex pair is observed (Figure 5), although not in all cases. Here, the time-averaged measurement of the meandering plume smears out the double peak (Figure 6, left panel). It can be shown that if a bimodal Gauss profile oscillates with an amplitude larger than 90% of the distance between both peaks, the double peak vanishes in the time-averaged profile. Due to the larger distance of its centre to the axis, the double vortex pair flow structure is clearly observed in most of the experiments (Figure 6). The horizontal distance of the center of the vortex is located at y/z = 0.3-0.5, which is in line with the observations by Diez *et al.* (2005). The observation of the position of the concentration maximum at y/z=0.2 in the ASM profiles is also in line with the work by the same authors.

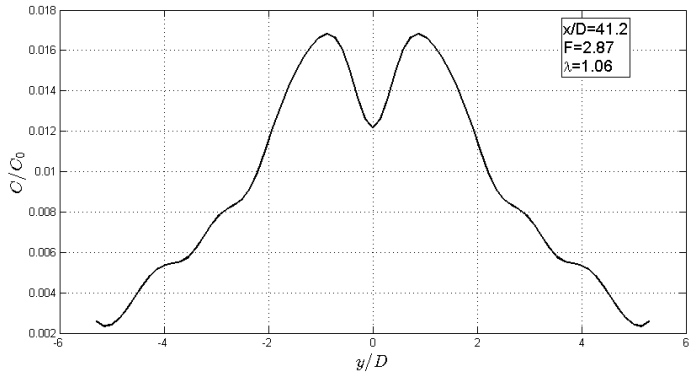

Figure 5. Sediment concentration profile measured using the ASM profiler at the vertical level of the concentration peak.

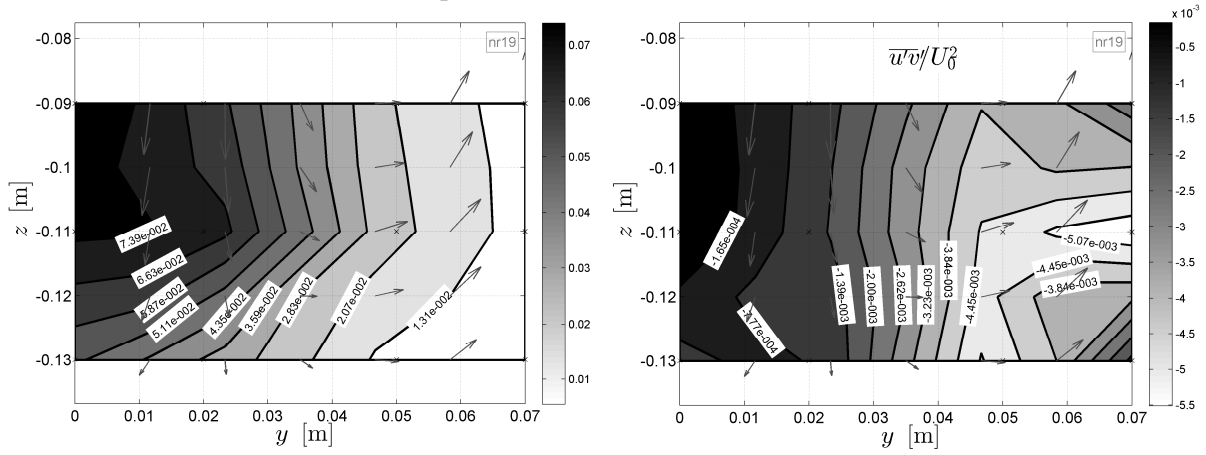

Figure 6.Lower-right quadrant of (left panel) the concentration profile C/C_0 and of (right panel) the lateral turbulent flux of horizontal momentum, with velocity vectors in the yz-plane showing a vortex.

3.3 Turbulent quantities

Turbulent fluxes of momentum and sediment have been determined. Lateral fluxes of horizontal ambient flow momentum into the plume –normalised with the square of the ambient flow velocity- show values of typically $5 \cdot 10^{-3}$ at the edge of the plume to 10^{-4} at the center of the plume (Figure 6, right panel).

Vertical turbulent fluxes of sediment at the lower edge of the plume are an order of magnitude higher than the lateral fluxes at the outer edges (Figure 7). Vertical fluxes are negative, outbound of the plume, while the lateral flux is bidirectional: outbound the plume in the outer parts and directed towards the center at the inner part. This behaviour is explained by the double peak due to which a dip in the concentration exists in the center of the plume.

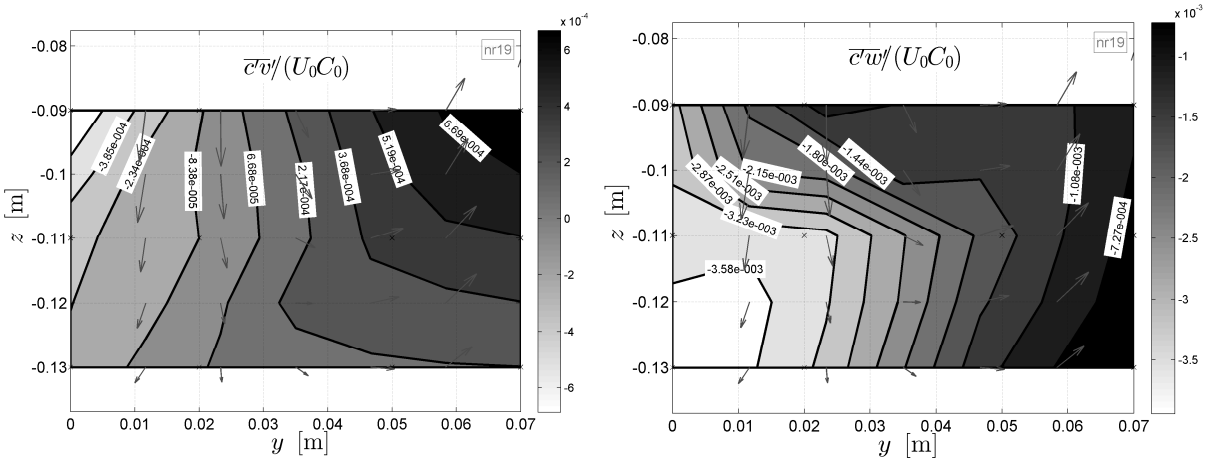

Figure 7.Lower-right quadrant of a vertical plume section: lateral (left panel) and vertical (right panel) turbulent flux of sediment, with velocity vectors in the *yz*-plane showing a vortex.

4. Discussion

Based on the two main characteristic numbers of buoyant jets or plumes in crossflow - Richardson number $Ri\ (=F_\Delta^{-2})$ and velocity ratio- a classification of the behavior of near-field buoyant jets issuing from a wall-mounted exit pipe is developed based on the angle of the plume axis in the bent plume regime, relatively far from the source. Plume showing limited or no vertical momentum after x/D=30 are categorized as horizontal plumes. Plumes having a slope of 1/5 or more after this distance are categorized as density currents. Intermediate cases are labeled in transitional regime.

When all 34 experiments are added to a diagram, an exponential function can be fitted forming the boundary between plume regimes (Figure 8). A density current is found under the condition $\lambda<\lambda_1(Ri)$, while a horizontal plume is found in case $\lambda>\lambda_2(Ri)$ and

$$\lambda_1 = a_1 e^{b_1 log_{10}(Ri)} \quad [3]$$

$$\lambda_2 = a_2 e^{b_2 log_{10}(Ri)} \quad [4]$$

where, a_1=1.14, b_1=0.64, a_2=2.26 and b_2=0.81.

It is clear that the coefficients will be in turn a function of the distance of the ship wake behind the pipe exit, which was in these experiments equal to 5 or 10 pipe diameters. In dredging vessel construction an overflow pipe at large distance from the stern is therefore advantageous for overflow plume containment. Moreover, when the vertical distance between

propeller wash and overflow plume is limited, the effect of this distance becomes even more important.

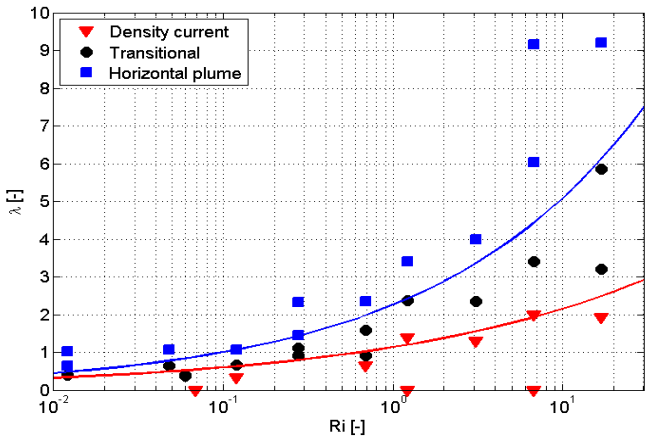

Figure 8.Plume regime diagram showing three zones.

5. Conclusions

Measurements of the structure of flow velocity and sediment concentration, as well as turbulent fluxes of momentum and sediment have been taken in a negatively buoyant sediment plume in crossflow, issued from a pipe mounted in a fixed plate.

The trajectory of the experimental buoyant plumes have been compared to integral laws and a Lagrangian model, showing agreement in plumes with low λ. Plumes formed by low density material in high background flow velocity differ most significantly from simple models. The plume behaviour is therefore influenced by the wake and boundary layer of the schematised polycarbonate ship hull where shear flow induces increased vertical mixing. Therefore a location of the plume axis closer to the surface is observed compared to integral laws.

At relatively close distance to the exit pipe, the background flow is perpendicular to the plume. This effect produces the radially symmetric pipe-flow profile to deform into two counter-rotating vortices. With this structure, the plume adopts a larger surface area leading to higher mixing and dilution rates.

A prediction of the plume regime has been developed for negatively buoyant plumes issued in a boundary layer. Based on a function of Richardson number and velocity ratio density current, transitional or horizontal plume regimes can be discriminated.

The experiments offer an extensive dataset on the mixing in this type of plumes, useful for calibration of a numerical model.

Acknowledgments

The author wishes to thank the “Instituut voor aanmoediging van Innovatie door Wetenschap en Technologie” (IWT) and International Marine and Dredging Consultants (IMDC) for funding this research project.

References

ARGUS Surface Meter: www.argusnet.de/Instruments/ASM/ASM-REFERENCE.PDF

Dankers, P.J.T., 2002. The behavior of fines released due to dredging. A literature review. Technical University of Delft, pp 59.

Diez, F.J., Bernal, L.P. and Faeth, G.M. (2005). PLIF and PIV measurements of the self-preserving structure of steady round buoyant turbulent plumes in crossflow. Int. J. of Heat and Fluid Flow 26. p873-882.

Decrop, B., De Mulder, T. and Toorman E., 2012. Mean and fluctuating suspended sediment concentration using ADV. Hydraulic Measurement and Experimental Method Conference, Utah, 2012.

Lee, J.H.W and Chu, V., 2003. Turbulent jets and Plumes: A Lagrangian approach. Kluwer, pp378.

Papanicolaou, P.N. and List, E.J., 1988. Investigations of round vertical turbulent buoyant jets. J. Fluid Mech. Vol 195, pp. 341-391.

Salehi, M. and Strom, K.B. (2009). Suspended sediment concentration measurements of muddy sediments with an ADV. World Environmental and Water Resources Congress 2009: Great Rivers, 3572-3577.

Salehi, M. and Strom, K.B. (2011). Using velocimeter signal to noise ratio as a surrogate measure of suspended mud concentration. Cont. Sh. Res. 31, 1020-1032. Elsevier.

Shabbir, A. and Taulbee, D.B., 2000. Experimental balances for the second moments for a buoyant plume and their implication on turbulence modelling. International Journal of Heat and Mass Transfer 43, 1777-1790.

Smith, G.G., Weitz, N., Soltau, C., Viljoen, A., Luger, S. and Maartens, L., 2008. Fate of fine sediment from dredger-based mining in a wave-dominated environment at Chameis Bay, Namibia. Journal of Coastal Research, 24(1), 232-247. West Palm Beach (Florida), ISSN 0749-0208.

Spearman, J., Bray, R.N., Land, J., Burt, T.N., Mead, C.T. and Scott, D., 2007. Plume dispersion modeling using dynamic representation of trailer dredger source terms. In: Estuarine and Coastal Fine Sediment Dynamics, p417-448. Proceeding in Marine Science. Elsevier.